Detecting long-duration cloud contamination in hyper-temporal NDVI imagery

Amjad Ali [a,b,*], C.A.J.M. de Bie [a], A.K. Skidmore [a]

[a] Faculty of Geo-Information Science and Earth Observation (ITC), University of Twente, Hengelosestraat 99, 7500 AE Enschede, The Netherlands
[b] Pakistan Space and Upper Atmosphere Research Commission (SUPARCO), SUPARCO Road, P.O. Box No. 8402, Karachi 75270, Pakistan

ARTICLE INFO

ABSTRACT

Cloud contamination impacts on the quality of hyper-temporal NDVI imagery and its subsequent interpretation. Short-duration cloud impacts are easily removed by using quality flags and an upper envelope filter, but long-duration cloud contamination of NDVI imagery remains. In this paper, an approach that goes beyond the use of quality flags and upper envelope filtering is tested to detect when and where long-duration clouds are responsible for unreliable NDVI readings, so that a user can flag those data as missing. The study is based on MODIS Terra and the combined Terra-Aqua 16-day NDVI product for the south of Ghana, where persistent cloud cover occurs throughout the year. The combined product could be assumed to have less cloud contamination, since it is based on two images per day. Short-duration cloud effects were removed from the two products through using the adaptive Savitzky–Golay filter. Then for each 'cleaned' product an unsupervised classified map was prepared using the ISODATA algorithm, and, by class, plots were prepared to depict changes over time of the means and the standard deviations in NDVI values. By comparing plots of similar classes, long-duration cloud contamination appeared to display a decline in mean NDVI below the lower limit 95% confidence interval with a coinciding increase in standard deviation above the upper limit 95% confidence interval. Regression analysis was carried out per NDVI class in two randomly selected groups in order to statistically test standard deviation values related to long-duration cloud contamination. A decline in seasonal NDVI values (growing season) were below the lower limit of 95% confidence interval as well as a concurrent increase in standard deviation values above the upper limit of the 95% confidence interval were noted in 34 NDVI classes. The regression analysis results showed that differences in NDVI class values between the Terra and the Terra-Aqua imagery were significantly correlated ($p < 0.05$) with the corresponding standard deviation values of the Terra imagery in case of all NDVI classes of two selected NDVI groups. The method successfully detects long-duration cloud contamination that results in unreliable NDVI values. The approach offers scientists interested in time series analysis a method of masking by area (class) the periods when pre-cleaned NDVI values remain affected by clouds. The approach requires no additional data for execution purposes but involves unsupervised classification of the imagery to carry out the evaluation of class-specific mean NDVI and standard deviation values over time.

1. Introduction

The availability of accurate land cover information is important for policy formulation and the management of natural resources, including biodiversity, forestry and the issue of food security (Cihlar, 2000; Defries and Belward, 2000). Climate change issues further enhance the general interest in the availability and use of accurate land use/land cover information at regional to global scales (Cihlar, 2000). The common method of generating land cover information is the use of satellite imagery (Cihlar, 2000; Lillesand et al., 2004). During the past decade Normalized Difference Vegetation Index (NDVI) time series imagery has increasingly been used for land use/land cover mapping and monitoring (Zhang et al., 2003; Xiao et al., 2006; Wardlow et al., 2007; Bontemps et al., 2008; Zhang et al., 2008; de Bie et al., 2011; Nguyen et al., 2011). NDVI provides a measure of photosynthetically active biomass (Sarkar and Kafatos, 2004). The available NDVI time series data suffer from cloud contamination, thus limiting the quality of the maps generated (Jonsson and Eklundh, 2002; Fensholt et al., 2006; Ma and Veroustraete, 2006; Hird and McDermid, 2009; Clark et al., 2010).

The presence of clouds and haze reduces the spectral reflectance in infra-red, causing reduced NDVI readings (Gu et al., 2009). To overcome contamination caused by clouds and atmospheric effects at data supplier level, the preprocessing routines for satellite data

* Corresponding author at: Faculty of Geo-Information Science and Earth Observation (ITC), University of Twente, Hengelosestraat 99, 7500 AE Enschede, The Netherlands. Tel.: +31 053 4874444; fax: +31 053 4874400.
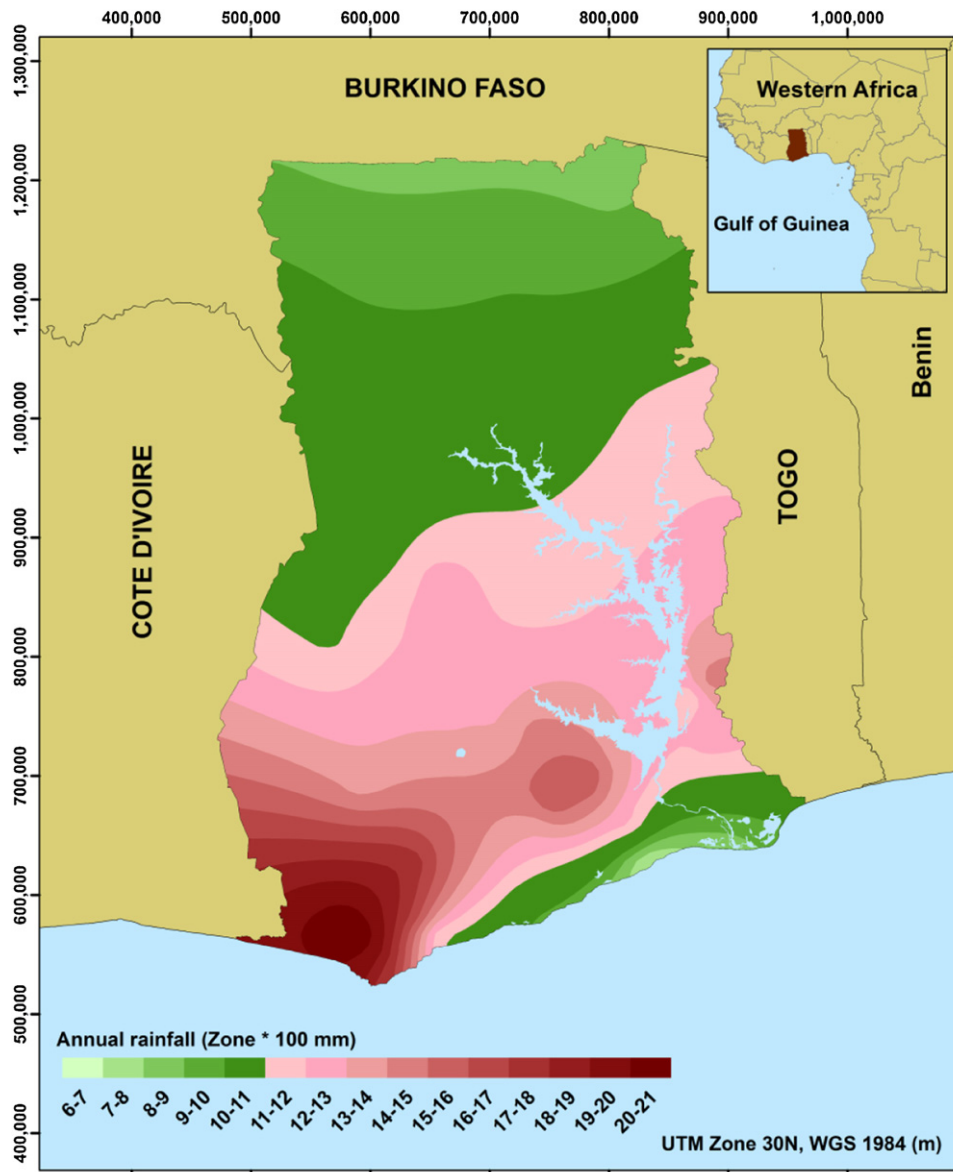E-mail addresses: amjad@itc.nl, amjadalee65@yahoo.com (A. Ali).

Fig. 1. Rainfall map of Ghana, showing spatial distribution of mean annual rainfall (1961–1997).
Source: Ghana Meteorological Services Department, Leigon, Ghana.

include the generation of quality flags, and maximum composite (MVC) imagery (Holben, 1986; Stowe et al., 1991). The remaining cloud corrections and adjustments are made at user level through the use of provided quality flags and data adjustment algorithms.

The quality flags provide pixel-level information about presence of atmospheric aerosols, cloud cover, presence of snow and ice cover, likelihood of shadow, and bidirectional reflectance (Stowe et al., 1991, 1999; Ackerman et al., 1998). At user level, they provide important information that serves to reduce the use of spurious NDVI data (Jonsson and Eklundh, 2002).

The maximum value composite technique (Holben, 1986; Stowe et al., 1991) selects the highest recorded value for each pixel during a pre-defined period of time. The technique has improved the overall data quality, reducing the effects of clouds and haze. However, in the tropics and some coastal regions where cloud cover persists for long duration, maximum value composite technique is known to be poor in dealing with cloud contamination (Holben, 1986; Goward et al., 1991; Verhoef et al., 1996; Cihlar et al., 1997; Roerink et al., 2000; Fensholt et al., 2010).

To adjust NDVI values affected by undetected clouds and those marked missing using quality flags, researchers have proposed a number of methods. These include best index slope extraction (BISE) (Viovy et al., 1992), the weighted least squares regression approach (Swets et al., 1999), geostatistical methods (Addink and Stein, 1999; Van der Meer, 2012), modified BISE filtering (Lovell and Graetz, 2001), Fourier analysis (Verhoef et al., 1996; Roerink et al., 2000; Moody and Johnson, 2001; Wagenseil and Samimi, 2006), mean value iteration (Ma and Veroustraete, 2006), function fitting approaches (adaptive Savitzky–Golay and logistics function fitting) (Jönsson and Eklundh, 2004), the whittaker smoother (Atzberger and Eilers, 2011b), wavelets (Lu et al., 2007) and iterative interpolation for data reconstruction (Julien and Sobrino, 2010). However, scientists have reported that, although they are able to adjust data affected by short-duration clouds, they are unable to correct the long-duration cloud contamination problem (Jonsson and Eklundh, 2002; Chen et al., 2004; Jönsson and Eklundh, 2004; Lu et al., 2007; Atzberger and Eilers, 2011a). The characterization of cloud duration as short or long is relative and changes with different correction tools applied; depending upon
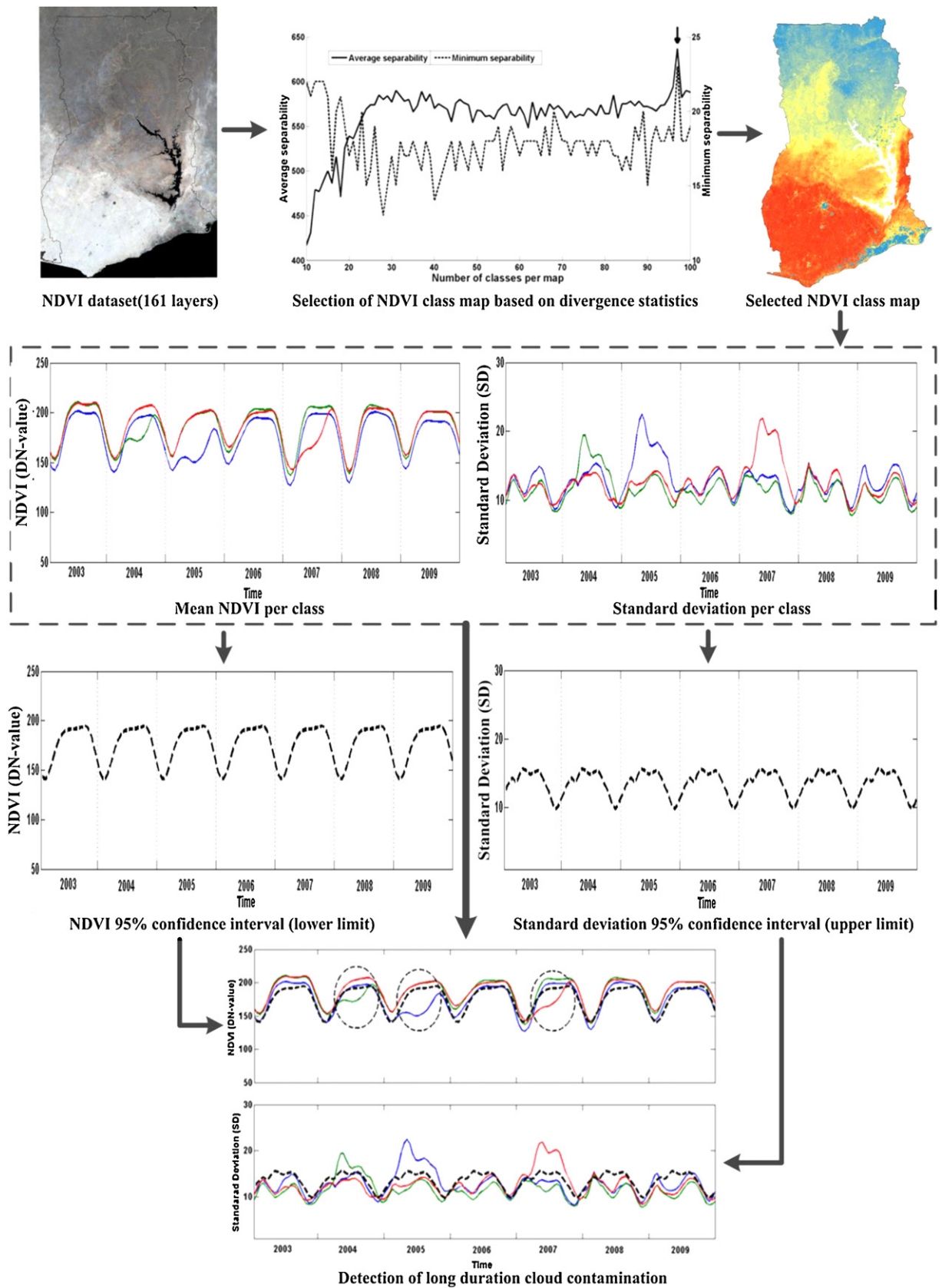
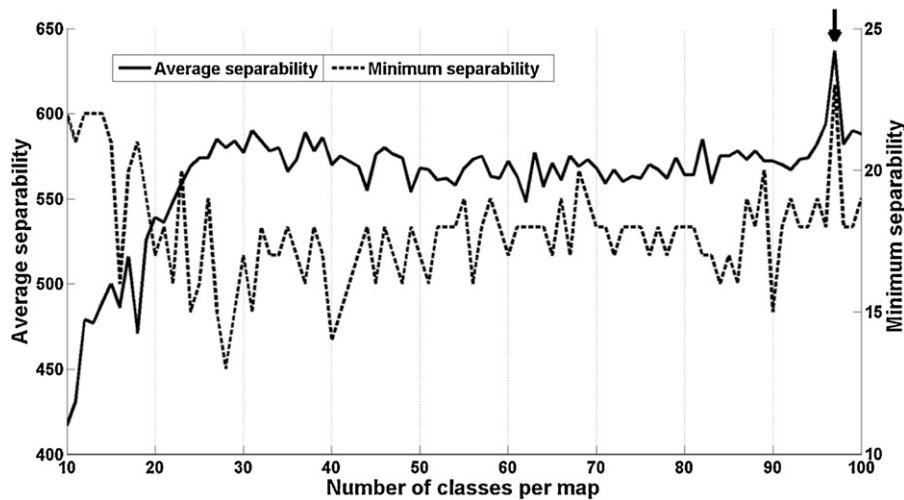**Fig. 2.** Schematic diagram of the method used.

Fig. 3. Average and minimum divergence statistics of maps with 10–100 classes. The arrow points to the coinciding peak in both separability values (97 classes).

their robustness to deal with data contamination resulted due to clouds.

The NDVI time series data affected by long-duration clouds reduce the quality of any subsequent interpretation. The authors recognized the need and aims to develop a procedure to detect which data are affected by long-duration cloud contamination particularly in the case of hyper-temporal NDVI time series. After detection, a user can flag those values as missing and avoid their use during subsequent analysis. The method builds on statistically derived unsupervised classification of the time series imagery.

2. Materials and methods

2.1. Study area

Ghana was selected as study area because of the high frequency of cloudy days (Fig. 1). It has a tropical savanna climate (Peel et al., 2007), with annual temperatures above 24 °C (Ghana Environmental Protection Agency, 2001). Ghana has two distinct rainfall regimes in two different parts of the country. Southern Ghana has a high frequency of cloudy days and receives more rainfall than the northern parts (Kakane and Sogaard, 1997; Shahin, 2002; Fensholt et al., 2007). Annual average rainfall varies from 600 to 2100 mm in the southern regions and is marked by two wet seasons: March–July, and September–November (Owusu et al., 2008). In northern Ghana, rainfall occurs in one season (May–October), with annual rainfall ranging from 700 to 1100 mm.

2.2. Data preprocessing

MODIS Terra (MOD13Q1) and MODIS Aqua (MYD13Q1) 16-day maximum value composite NDVI imagery with a 250 m spatial resolution was downloaded from https://wist.echo.nasa.gov/wist-bin (accessed February 2010). The imagery covered the period from 1 January 2003 to 31 December 2009.

Terra and Aqua sensors acquire images at two different times of the day (Terra 10:30 am and Aqua 01:30 pm local standard time). The downloaded Terra and Aqua 16-day maximum value composite imagery has similar spatial, spectral and radiometric characteristics. NDVI values of Terra and Aqua are reported to be strongly correlated ($R^2 = 0.97$, RMSE = 0.04) (Gallo et al., 2005).

The Vegetation Index Quality (VIQ) layers provide pixel values affected by clouds, haze and other atmospheric effects, which were used to set the value of those pixels to missing. All NDVI values

were transformed to DN values (0–255) using Eq. (1), where DN = 0 is coded as missing.

$$NDVI(DN - value) = integer_{16\text{-bit signed}} \text{ of } NDVI * 0.02133 + 43.117 \tag{1}$$

The Terra-Aqua dataset was generated by combining both Terra and Aqua maximum value composite NDVI imagery. The combined dataset was expected to suffer less from cloud contamination because it is based on two images a day instead of one.

Pixel-specific date stamps were used to combine the two images. They have an 8-day difference in the start dates of their 16-day maximum value composite periods, meaning that an 8-day shift between the two imagery series occurred. We retained the Terra 16-day period as default when merging the Aqua data. Using pixel-specific date stamps, the pixel-specific Aqua values were compared with the corresponding maximum value composite values of the Terra imagery; the highest values (maximum composite) were kept to represent the relevant Terra period and pixel.

Finally, the adaptive Savitzky–Golay method built in TIMESAT was used to remove short-duration impacts on cloud-affected pixel values of the Terra and Terra-Aqua NDVI datasets (Jönsson and Eklundh, 2004; Beltran-Abaunza, 2009). This method is widely used and found useful for noisy and non-uniform NDVI time series datasets (Jönsson and Eklundh, 2004; Feng et al., 2008; Beltran-Abaunza, 2009; Boschetti et al., 2009).

2.3. Long-duration cloud contamination detection

The preprocessed Terra hyper-temporal NDVI dataset, composed of 161 layers, was classified into 10–100 classes using the Iterative Self-Organizing Data Analysis (ISODATA) algorithm (Ball and Hall, 1965; Tou and Gonzalez, 1974). ISODATA is used for an unsupervised classification of patterns in remote sensing into clusters or classes (Jain et al., 1999). It is iterative and self-organizing, which repeats itself and locates classes with minimum user input (Tou and Gonzalez, 1974; Swain and Davis, 1978). No prior knowledge is needed to train the processing. This has more consistent results and easy to reproduce. Similarly different forms of statistics such as divergence statistics; Jeffries-Matsushita can be calculated for each class to finally select the optimum classification result (de Bie et al., 2012).

The ISODATA algorithm was run with the convergence threshold set to 1 and iterations set to 50. After classification, the average and minimum divergence values between cluster centroids were plotted against the number of classes generated. Coinciding high average and minimum divergence values were used as guidance
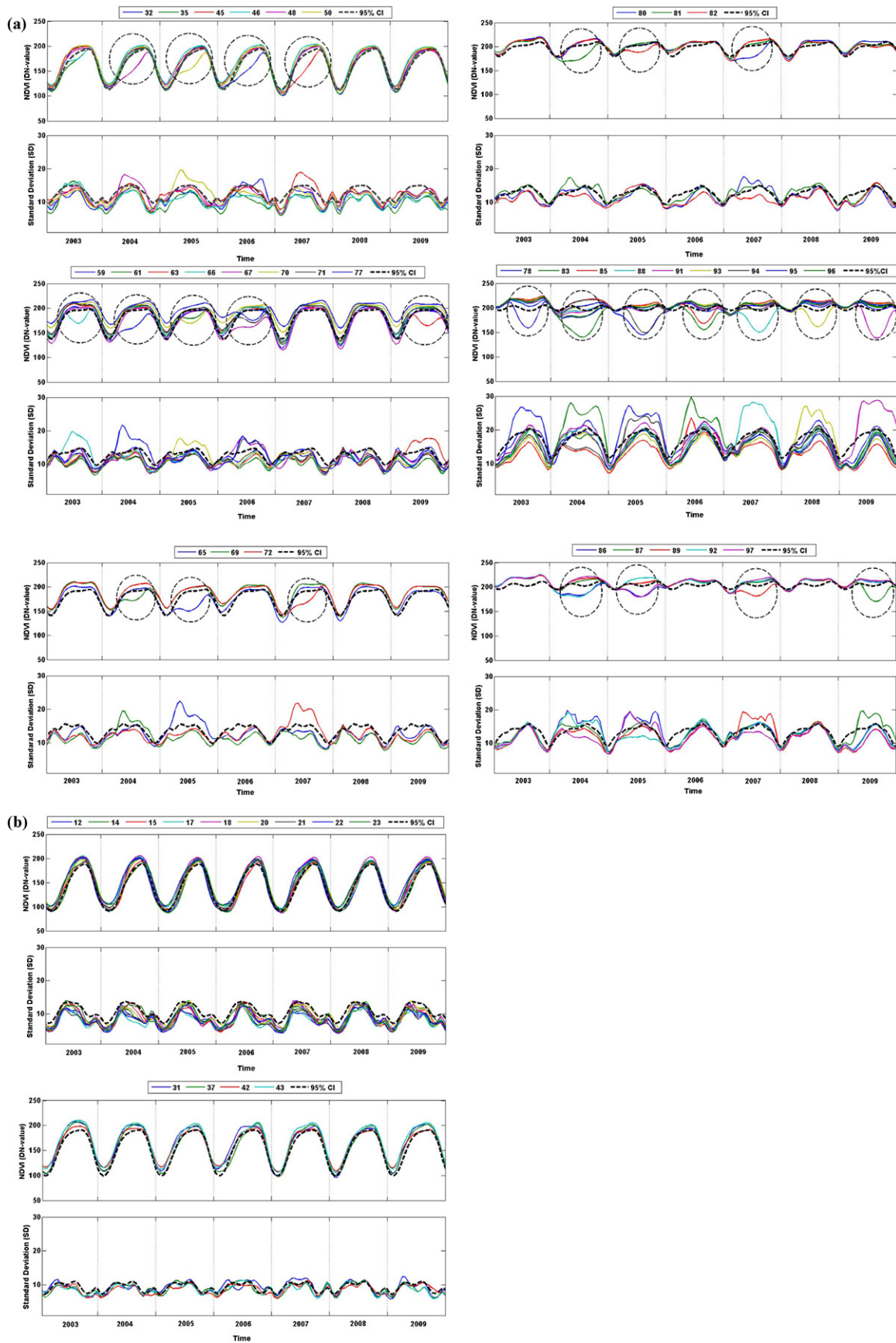
Fig. 4. Terra-derived NDVI class profiles arranged in groups: (a) characterized by suspicious decline in NDVI values during the growing season (marked with circles) and (b) two groups of NDVI class profiles showing no suspicious decline in NDVI values. 1-sided 95% confidence interval (95% CI) is shown in dashed line.
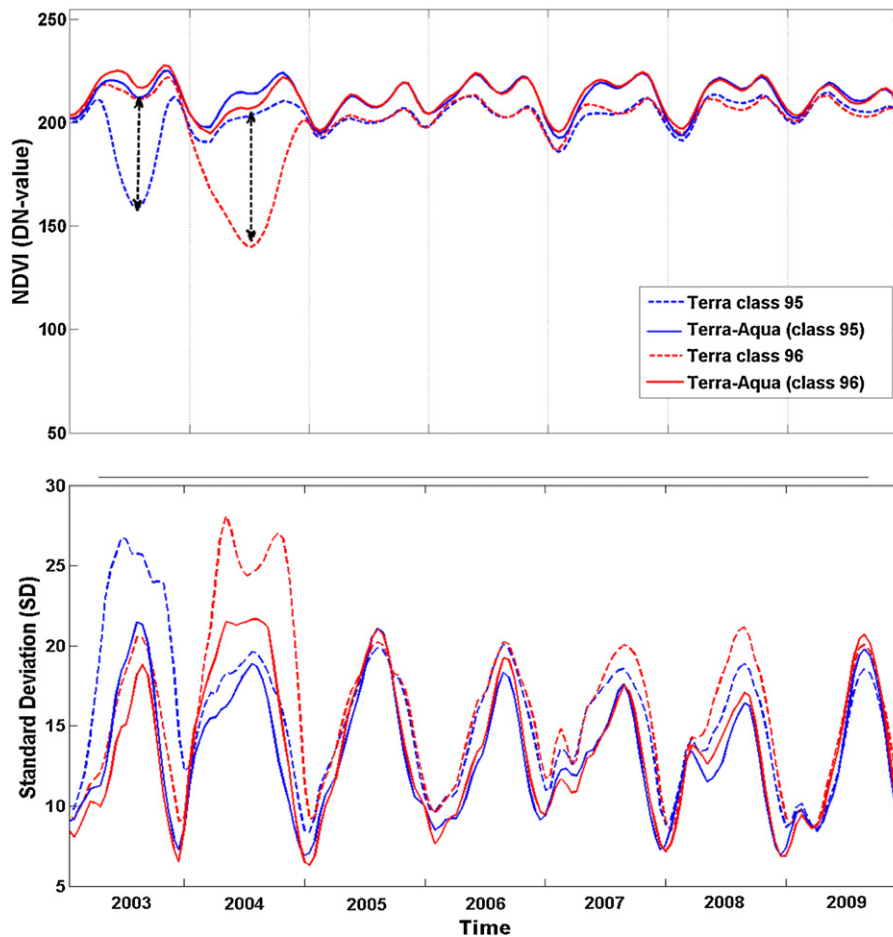
Fig. 5. Comparison of NDVI and standard deviation profiles of the selected two classes derived from the Terra and Terra-Aqua products. The classes of each product cover similar areas in southern Ghana.

to select the optimal classified image (Swain and Davis, 1978). The statistics generated by the ISODATA algorithm for selected NDVI classes were used to detect areas affected by long-duration cloud contamination.

NDVI profiles representing the mean NDVI values of all the pixels of the respective class were plotted over time (2003–2009) to visualize their temporal behavior, and based on shape and intensity the NDVI profiles were assigned to different groups.

The mean NDVI 95% confidence interval lower limit and the standard deviation 95% confidence interval upper limit were calculated to objectively define cloud contamination in NDVI values. To calculate the lower limit of the 95% confidence interval of NDVI, first the mean annual NDVI profiles (23 values) were calculated by averaging each decade from 2003 to 2009. After that a single mean NDVI profile of all the classes in a group was created and used as a reference for calculating the lower limit 95% confidence interval for that group. The mean profile of all the classes portrayed the normal behavior of all the classes in a group and was used as a reference for defining a suspicious decline. Similarly the standard deviation values of each class in a group were first averaged (pooled standard deviation) on decadal basis across the years (2003–2009) to create a mean profile of each class (23 values) in a group. They were then averaged (pooled standard deviation) per group to create a single standard deviation profile as a reference to find an upper limit 95% confidence interval of standard deviation values. The 95% confidence interval is used to indicate a statistically safe range within which a value can be considered closer to the actual values (Burns and Burns, 2008). The upper limit 95% confidence

interval of standard deviation values was used because cloud contamination negatively affects NDVI values therefore increases the standard deviation values (Fig. 2).

To identify long-duration cloud contamination within a group of NDVI profiles, the NDVI and standard deviation profile of each class within that group were plotted. The mean NDVI 95% confidence interval lower limit and the standard deviation 95% confidence interval upper limit were added to the NDVI standard deviation plots. A decline in NDVI value below the lower limit of the 95% confidence interval and a concurrent increase in standard deviation above the upper limit of the 95% confidence interval indicate long-duration cloud contamination.

2.4. Validation

Two groups of Terra-NDVI classes with a suspicious decline in NDVI values were randomly chosen for the validation analysis. Firstly, the level of differences between NDVI values extracted from Terra and Terra-Aqua NDVI imagery was inspected by comparing two NDVI classes from one of the selected group. It was checked to see whether the period showing high differences between the two imagery products coincided with an increase in the standard deviation values of the Terra-based NDVI classes.

Secondly, regression analyses were carried out per NDVI class to statistically test whether standard deviation values related to long-duration cloud contamination. The analysis was performed using the differences in the NDVI values of the Terra and
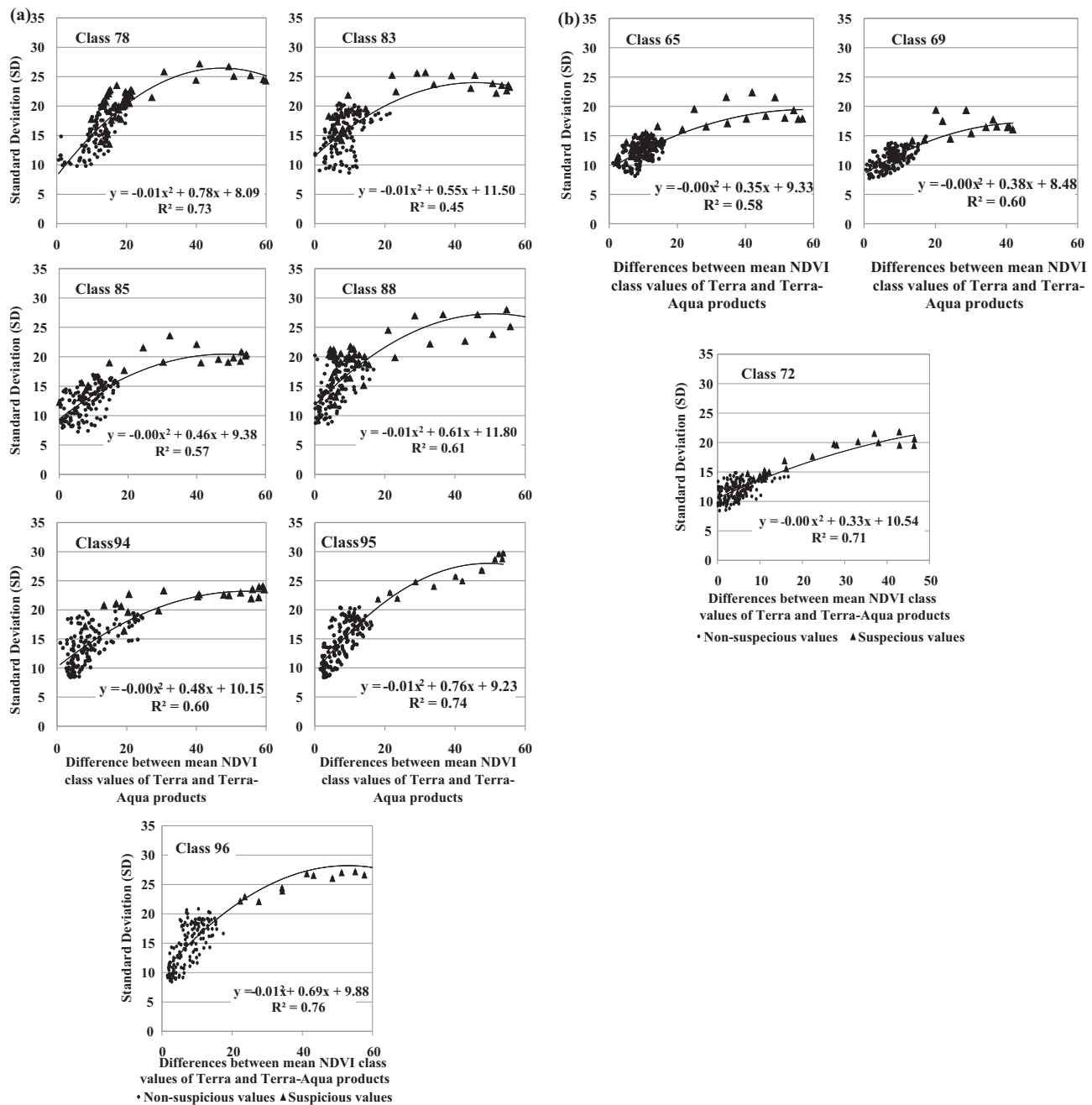
Fig. 6. Scatterplots showing relationship between differences in NDVI of Terra and Terra-Aqua products and the standard deviation derived from the Terra product of two randomly selected groups of NDVI classes.

Terra-Aqua products versus the standard deviation values of the Terra product for all the NDVI classes in the two selected groups.

3. Results

3.1. Long-duration cloud contamination detection

Using the ISODATA algorithm, the preprocessed Terra dataset was classified into maps with 10–100 NDVI classes. Divergence statistics revealed a high average separability for the 97-class map, coinciding with a peak in minimum divergence statistics (Fig. 3). The 97-class map was selected as the optimal classification result. This map and derived statistics were used onwards for detecting long-duration cloud contamination.

The NDVI and standard deviation plots were organized in groups on the basis of comparable temporal behavior, as shown in Fig. 4. NDVI class profiles of those classes showing a decline in seasonal NDVI values (growing season) below the lower limit of the 95% confidence interval as well as a concurrent increase in standard deviation values above the upper limit of the 95% confidence interval (marked with circles) were found having suspicious NDVI values (Fig. 4a). These long term drops in NDVI values were considered suspicious because they were not consistent with the historical trends of the classes in same group and it is unlike the annual growth and the decline periods of vegetation of the same group. Similarly high increase in standard values indicates spread of NDVI values, which may be associated with cloud contamination. Similarly high standard deviation values show spread of data values and
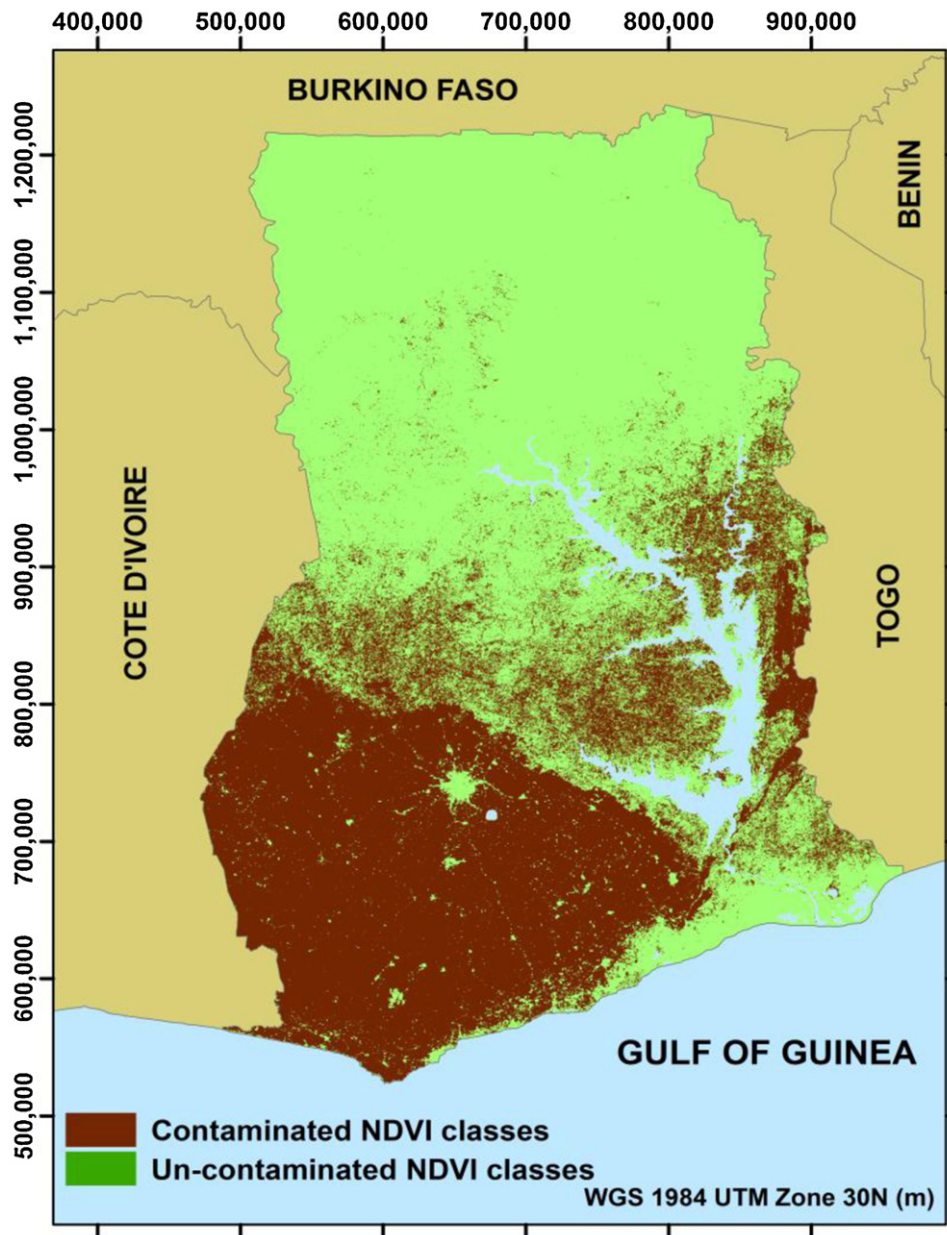
Fig. 7. The spatial distribution of contaminated and uncontaminated NDVI classes.

hence make it suspicious. Fig. 4a shows 34 NDVI classes found with suspicious NDVI values. These NDVI classes were located mainly in the annual average rainfall zone of 1200–2100 mm (Figs. 1 and 7).

Compared with Fig. 4a, groups of the NDVI classes that have a consistent behavior over time as well as a mean NDVI value that does not decline below the NDVI 95% confidence interval experienced no sharp increase in standard deviation values above the upper limit of the 95% confidence interval (Fig. 4b). These NDVI classes have smooth and consistent historical trends as compared to profiles of NDVI classes shown in Fig. 4a. Fig. 4b shows only two randomly selected NDVI groups which have no suspicious NDVI values. They occur mainly in drier northern zones with less than 1200 mm rainfall (Fig. 1). The spatial distribution of the NDVI classes is shown in Fig. 7.

3.2. Validation

The differences between the NDVI values of the Terra and Terra-Aqua products became large with the decline in

seasonal Terra NDVI. The Terra-Aqua profiles do not display such seasonal decline and synchronous sharp increase in standard deviation values (Fig. 5). It also showed that declines were not related to actual changes in greenness of present land cover but rather to long-duration cloud cover.

Regression analysis results given in Fig. 6 showed that the NDVI difference in the Terra product, compared with the Terra-Aqua product, was significantly ($p < 0.05$) correlated with the standard deviation values of the Terra product. The R^2 values of 0.73, 0.45, 0.57, 0.61, 0.60, 0.74 and 0.76 was found in case of NDVI classes 78, 83, 85, 88, 94, 95 and 96, respectively (Fig. 6a). Similarly the second group of NDVI classes (65, 69 and 72) recorded R^2 of 0.58, 0.60 and 0.71, respectively (Fig. 6b). From Fig. 6 it can also be deduced that standard deviation values above a 95% confidence interval upper limit relate to cloud contamination, as discriminated by NDVI classes showing decline in seasonal NDVI values below a 95% confidence interval lower limit.

4. Discussion

This study has introduced an exploratory method that detects long-duration cloud contamination that in turn results in unreliable NDVI values. The method presented in this article requires no additional source of information or external data for execution purposes but requires the unsupervised classification of the imagery to carry out the evaluation of class-specific mean NDVI and standard deviation values over the time. Including this method in the preprocessing routines of NDVI time series data can help to avoid the use of anomalous NDVI data in time series studies. The method can be applied to any type of time series data, irrespective of spatial and temporal variations. The method is simple to implement and reproduce. This technique can be beneficial for NDVI spectro-temporal analysis based land use/land cover mapping and monitoring, particularly in the tropics.

A synchronous decline in seasonal NDVI values below a lower limit 95% confidence interval and an increase in the standard deviation above an upper limit 95% confidence interval indicate possible long-term cloud contamination that was not removed by preprocessing routines. From Fig. 4 it is obvious that the decline in NDVI, which is linked to an increase in standard deviation values above the threshold (95% confidence interval), marks the periods when the NDVI values are affected by long-duration cloud cover. This is also proved in the regression analysis, which shows a positive and linear relation between differences in the Terra and Terra-Aqua imagery products versus standard deviation values of the Terra imagery (Fig. 6). The use of the 1-sided 95% confidence interval helps to objectively define the contamination. This also eliminates the short time effects in NDVI values unrelated to long-term missing data.

The validation using regression analysis to compare standard deviation and differences between the Terra and Terra-Aqua products was undertaken because standard deviation is considered the most common indicator to explain spread of data values (Myers, 1997). The Terra-Aqua product suffers less from cloud contamination, since it is a combination of two images per day. Fensholt et al. (2006) also used differences between Terra and Aqua as proxy for cloud cover. However, it is also notable that standard deviation alone can mislead interpretations because standard deviation normally increases in summer and decreases in winter owing to contrast in the reflectance of vegetation and soil (Gonza'Lez Loyarte and Menenti, 2000; Loyarte and Menenti, 2008). It is also clear from the results that the coinciding of seasonal decline in observed NDVI with increased standard deviation readings is suspicious.

This is the first study if its kind that successfully attempts to detect long-duration cloud contamination affects in hypertemporal NDVI imagery. In contrast, the available cloud contaminated data correction techniques are unable to correct long data gaps due to the inherent limitations associated with the models used (Holben, 1986; Swets et al., 1999; Jonsson and Eklundh, 2002; Fensholt et al., 2007; Lu et al., 2007; Gu et al., 2009; Hird and McDermid, 2009; Julien and Sobrino, 2010). By including this method in the preprocessing routines of NDVI time series analysis can help to mark the period and location of long-duration cloud contaminated NDVI values, which can be avoided in subsequent data analysis.

The spatial distribution of cloud-contaminated NDVI classes over an areas receiving more rainfall (>1200 mm) signify that areas receiving more rainfall and cloud cover experienced cloud contamination. More prevalent rainfall in southern Ghana is also reported by Kakane and Sogaard (1997), Fensholt et al. (2006, 2007). While in contrast those NDVI classes having no obvious contamination problem are distributed through northern Ghana, which is drier region with less chances of persistent cloud cover (Figs. 1 and 7).

5. Conclusion

In this paper a simple exploratory method is introduced to detect long-duration cloud contamination effects in hyper temporal NDVI imagery analysis. This is an approach, that goes beyond the use of quality flags and upper envelope filtering is tested to detect when and where long-duration clouds are responsible for unreliable NDVI readings. The approach offers the scientists interested in time series analysis, a method of masking by area (class) the periods when pre-cleaned NDVI values remain affected by clouds. It requires no additional data for execution purpose but involves unsupervised classification of the imagery to carry out the evaluation of class-specific mean NDVI and standard deviation values over the time. The method was validated with secondary dataset; however, in future real cloud cover data should be used for validation. The method will be useful for time series imagery based land cover mapping and monitoring specifically in areas where cloud cover is prevalent such as tropics.

References

Ackerman, S.A., Strabala, K.I., Menzel, W.P., Frey, R.A., Moeller, C.C., Gumley, L.E., 1998. Discriminating clear sky from clouds with MODIS. Journal of Geophysical Research 103, 32141–32157.

Addink, E.A., Stein, A., 1999. A comparison of conventional and geostatistical methods to replace clouded pixels in NOAA–AVHRR images. International Journal of Remote Sensing 20, 961–977.

Atzberger, C., Eilers, P.H.C., 2011a. Evaluating the effectiveness of smoothing algorithms in the absence of ground reference measurements. International Journal of Remote Sensing 32, 3689–3709.

Atzberger, C., Eilers, P.H.C., 2011b. A time series for monitoring vegetation activity and phenology at 10-daily time steps covering large parts of South America. International Journal of Digital Earth 4, 365–386.

Ball, G.H., Hall, D.J., 1965. Isodata: A Method of Data Analysis and Pattern Classification. Stanford Research Institute, Menelo Park, CA, United States.

Beltran-Abaunza, J.M., 2009. Method Development to Process Hyper-temporal Remote Sensing (RS) Images for Change Mapping. University of Twente, Enschede, The Netherlands.

Bontemps, S., Bogaert, P., Titeux, N., Defourny, P., 2008. An object-based change detection method accounting for temporal dependences in time series with medium to coarse spatial resolution. Remote Sensing of Environment 112, 3181–3191.

Boschetti, M., Stroppiana, D., Brivio, P.A., Bocchi, S., 2009. Multi-year monitoring of rice crop phenology through time series analysis of MODIS images. International Journal of Remote Sensing 30, 4643–4662.

Burns, R., Burns, R.P., 2008. Business Research Methods and Statistics Using SPSS. SAGE Publications, London.

Chen, J., Jönsson, P., Tamura, M., Gu, Z., Matsushita, B., Eklundh, L., 2004. A simple method for reconstructing a high-quality NDVI time-series data set based on the Savitzky–Golay filter. Remote Sensing of Environment 91, 332–344.

Cihlar, J., 2000. Land cover mapping of large areas from satellites: status and research priorities. International Journal of Remote Sensing 21, 1093–1114.

Cihlar, J., Ly, H., Li, Z., Chen, J., Pokrant, H., Huang, F., 1997. Multitemporal, multichannel AVHRR data sets for land biosphere studies – artifacts and corrections. Remote Sensing of Environment 60, 35–57.

Clark, M.L., Aide, T.M., Grau, H.R., Riner, G., 2010. A scalable approach to mapping annual land cover at 250 m using MODIS time series data: a case study in the Dry Chaco ecoregion of South America. Remote Sensing of Environment 114, 2816–2832.

de Bie, C.A.J.M., Khan, M.R., Smakhtin, V.U., Venus, V., Weir, M.J.C., Smaling, E.M.A., 2011. Analysis of multi-temporal SPOT NDVI images for small-scale land-use mapping. International Journal of Remote Sensing 32, 6673–6693.

de Bie, C.A.J.M., Nguyen, T.T.H., Ali, A., Scarrott, R., Skidmore, A.K., 2012. LaHMa: a landscape heterogeneity mapping method using hyper-temporal datasets. International Journal of Geographical Information Science 26, 1–16.

Defries, R.S., Belward, A.S., 2000. Global and regional land cover characterization from satellite data: an introduction to the Special Issue. International Journal of Remote Sensing 21, 1083–1092.

Feng, G., Morisette, J.T., Wolfe, R.E., Ederer, G., Pedelty, J., Masuoka, E., Myneni, R., Bin, T., Nightingale, J., 2008. An algorithm to produce temporally and spatially continuous MODIS-LAI time series. IEEE Geoscience and Remote Sensing Letters 5, 60–64.

Fensholt, R., Anyamba, A., Stisen, S., Sandholt, I., Park, E., Small, J., 2007. Comparisons of compositing period length for vegetation index data from polar-orbiting and geostationary satellites for the cloud-prone region of West Africa. Photogrammetric Engineering and Remote Sensing 73, 297–309.

Fensholt, R., Sandholt, I., Proud, S.R., Stisen, S., Rasmussen, M.O., 2010. Assessment of MODIS sun-sensor geometry variations effect on observed NDVI using MSG SEVIRI geostationary data. International Journal of Remote Sensing 31, 6163–6187.

Fensholt, R., Sandholt, I., Stisen, S., Tucker, C., 2006. Analysing NDVI for the African continent using the geostationary meteosat second generation SEVIRI sensor. Remote Sensing of Environment 101, 212–229.

Gallo, K., Ji, L., Reed, B., Eidenshink, J., Dwyer, J., 2005. Multi-platform comparisons of MODIS and AVHRR normalized difference vegetation index data. Remote Sensing of Environment 99, 221–231.

Ghana Environmental Protection Agency, 2001. Ghana's Initial National Communications Report under the United Nations Framework Convention on Climate Change. Accra, Ghana.

Gonza' Lez Loyarte, M.M., Menenti, M., 2000. Usefulness of Fourier parameters to detect regional and local droughts within a time series of NOAA/AVHRR-NDVI data (GAC). In: Roerink, G.J., Menenti, M. (Eds.), Time Series of Satellite Data: Development of New Products. Netherlands Remote Sensing Board, Wageningen, pp. 63–70.

Goward, S.N., Markham, B., Dye, D.G., Dulaney, W., Yang, J., 1991. Normalized difference vegetation index measurements from the advanced very high resolution radiometer. Remote Sensing of Environment 35, 257–277.

Gu, J., Li, X., Huang, C., Okin, G.S., 2009. A simplified data assimilation method for reconstructing time-series MODIS NDVI data. Advances in Space Research 44, 501–509.

Hird, J.N., McDermid, G.J., 2009. Noise reduction of NDVI time series: An empirical comparison of selected techniques. Remote Sensing of Environment 113, 248–258.

Holben, B.N., 1986. Characteristics of maximum-value composite images from temporal AVHRR data. International Journal of Remote Sensing 7, 1417–1434.

Jain, A.K., Murty, M.N., Flynn, P.J., 1999. Data clustering: a review. ACM Computing Surveys (CSUR) 31, 264–323.

Jonsson, P., Eklundh, L., 2002. Seasonality extraction by function fitting to time-series of satellite sensor data. IEEE Transactions on Geoscience and Remote Sensing 40, 1824–1832.

Jönsson, P., Eklundh, L., 2004. TIMESAT – a program for analyzing time-series of satellite sensor data. Computers and Geosciences 30, 833–845.

Julien, Y., Sobrino, J.A., 2010. Comparison of cloud-reconstruction methods for time series of composite NDVI data. Remote Sensing of Environment 114, 618–625.

Kakane, V.C.K., Sogaard, H., 1997. Estimation of surface temperature and rainfall in Ghana Geografisk Tidsskrift. Danish Journal of Geography 97, 76–85.

Lillesand, T.M., Kiefer, R.W., Chipman, J.W., 2004. Remote Sensing and Image Interpretation, 5th ed. John Wiley and Sons, USA.

Lovell, J.L., Graetz, R.D., 2001. Filtering Pathfinder AVHRR Land NDVI data for Australia. International Journal of Remote Sensing 22, 2649–2654.

Loyarte, M.M.G., Menenti, M., 2008. Impact of rainfall anomalies on Fourier parameters of NDVI time series of northwestern Argentina. International Journal of Remote Sensing 29, 1125–1152.

Lu, X., Liu, R., Liu, J., Liang, S., 2007. Removal of noise by wavelet method to generate high quality temporal data of terrestrial MODIS products. Photogrammetric Engineering and Remote Sensing 73, 1129–1139.

Ma, M., Veroustraete, F., 2006. Reconstructing pathfinder AVHRR land NDVI time-series data for the Northwest of China. Advances in Space Research 37, 835–840.

Moody, A., Johnson, D.M., 2001. Land-surface phenologies using the discrete Fourier transform. Remote Sensing of Environment 75, 305–323.

Myers, J.C., 1997. Geostatistical Error Management: Quantifying Uncertainty for Environmental Mapping. Van Nostrand Reinhold, New York.

Nguyen, T.T.H., de Bie, C.A.J.M., Ali, A., Smaling, E.M.A., Chu, T.H., 2011. Mapping the irrigated rice cropping patterns of the Mekong delta, Vietnam, through hyper-temporal SPOT NDVI image analysis. International Journal of Remote Sensing 33, 415–434.

Owusu, K., Waylen, P., Qiu, Y., 2008. Changing rainfall inputs in the Volta basin: implications for water sharing in Ghana. GeoJournal 71, 201–210.

Peel, M.C., Finlayson, B.L., McMahon, T.A., 2007. Updated world map of the Koppen–Geiger climate classification. Hydrology and Earth System Sciences 11, 1633–1644.

Roerink, G.J., Menenti, M., Verhoef, W., 2000. Reconstructing cloudfree NDVI composites using Fourier analysis of time series. International Journal of Remote Sensing 21, 1911–1917.

Sarkar, S., Kafatos, M., 2004. Interannual variability of vegetation over the Indian sub-continent and its relation to the different meteorological parameters. Remote Sensing of Environment 90, 268–280.

Shahin, M., 2002. Hydrology and Water Resources of Africa. Kluwer Academic, Dordrecht, Netherlands.

Stowe, L.L., Davis, P.A., McClain, E.P., 1999. Scientific basis and initial evaluation of the CLAVR-1 Global Clear/Cloud Classification Algorithm for the Advanced Very High Resolution Radiometer. Journal of Atmospheric and Oceanic Technology 16, 656–681.

Stowe, L.L., McClain, E.P., Carey, R., Pellegrino, P., Gutman, G.G., Davis, P., Long, C., Hart, S., 1991. Global distribution of cloud cover derived from NOAA/AVHRR operational satellite data. Advances in Space Research 11, 51–54.

Swain, P.H., Davis, S.M., 1978. Remote Sensing: The Quantitative Approach. McGraw-Hill, New York.

Swets, D.L., Reed, B.C., Rowland, J.D., Marko, S.E., 1999. A weighted least-squares approach to temporal NDVI smoothing. In: Proceedings of the 1999 ASPRS Annual Conference, Portland, Oregon.

Tou, J.T., Gonzalez, R.C., 1974. Pattern Recognition Principles. Addison-Wesley, Reading MA.

Van der Meer, F., 2012. Remote-sensing image analysis and geostatistics. International Journal of Remote Sensing 33, 5644–5676.

Verhoef, W., Menenti, M., Azzali, S., 1996. A colour composite of NOAA–AVHRR–NDVI based on time series analysis (1981–1992). International Journal of Remote Sensing 17, 231–235.

Viovy, N., Arino, O., Belward, A.S., 1992. The Best Index Slope Extraction (BISE): a method for reducing noise in NDVI time-series. International Journal of Remote Sensing 13, 1585–1590.

Wagenseil, H., Samimi, C., 2006. Assessing spatio-temporal variations in plant phenology using Fourier analysis on NDVI time series: results from a dry savannah environment in Namibia. International Journal of Remote Sensing 27, 3455–3471.

Wardlow, B.D., Egbert, S.L., Kastens, J.H., 2007. Analysis of time-series MODIS 250 m vegetation index data for crop classification in the U.S. Central Great Plains. Remote Sensing of Environment 108, 290–310.

Xiao, X., Boles, S., Frolking, S., Li, C., Babu, J.Y., Salas, W., Moore III, B., 2006. Mapping paddy rice agriculture in South and Southeast Asia using multi-temporal MODIS images. Remote Sensing of Environment 100, 95–113.

Zhang, X., Friedl, M.A., Schaaf, C.B., Strahler, A.H., Hodges, J.C.F., Gao, F., Reed, B.C., Huete, A., 2003. Monitoring vegetation phenology using MODIS. Remote Sensing of Environment 84, 471–475.

Zhang, X., Sun, R., Zhang, B., Tong, Q., 2008. Land cover classification of the North China plain using MODIS_EVI time series. ISPRS Journal of Photogrammetry and Remote Sensing 63, 476–484.